Unexpectedly low indentation strength of WB_{3} and MoB_{3} from first principles

Chenpeng Zang, Hong Sun, and Changfeng Chen

Phys. Rev. B **86**, 180101 — Published 8 November 2012

DOI: 10.1103/PhysRevB.86.180101

Unexpectedly low indentation strength of WB_3 and MoB_3 from first principles

Chenpeng Zang,[1] Hong Sun,[1,*] and Changfeng Chen[2,†]

[1]*Department of Physics, Shanghai Jiao Tong University, Shanghai 200240, and Key Laboratory of Artificial Structures and Quantum Control, Ministry of Education, China*
[2]*Department of Physics and High Pressure Science and Engineering Center, University of Nevada, Las Vegas, Nevada 89154, USA*

(Dated: October 28, 2012)

Recently synthesized WB_4 has attracted great interest because it exhibits the highest micro-indentation hardness among transition-metal light-element compounds. Latest theoretical studies [see, e.g., Phys. Rev. Lett. **108**, 255502 (2012)] show, however, that the previously assigned WB_4 structure is unstable; a WB_3 structure was proposed as an alternative structural model. Here we show by first-principles calculations that the pressure beneath the indenter drives a lateral bond and volume expansion in the proposed WB_3 and related MoB_3 structures, resulting in an unexpectedly low indentation strength to a level well below that of ReB_2. This is in direct contradiction to experimental results that show WB_4 has higher indentation hardness compared to ReB_2. Moreover, the calculated normalized c/a ratio of the WB_3 (and MoB_3) exhibits a negative pressure dependence, which is inconsistent with the experimentally observed trend. We therefore conclude that the proposed WB_3 structure is incompatible with experimental results and that the question of the crystal structure of the synthesized (nominal) WB_4 must be reopened for further study.

PACS numbers: 62.20.-x, 81.40.Jj, 61.50.Ah

Recent years have seen a surge in research of a new class of super- or ultra-hard materials by combining small, light covalent elements (B, C, N and O) with large, electron-rich transition metals (W, Re, Os, Ru, Ir, Pt, $\cdots$) because they offer a more cost-effective and versatile alternative to traditional superhard materials like diamond and cubic boron nitride that require high-pressure and high-temperature synthesis conditions[1]. Recent synthesis of rhenium diboride (ReB_2) at ambient pressure has ignited great interest in this class of metallic ultra-incompressible materials, leading to the reports on OsB_2[2], ReB_2[3–8], RuB_2[6], PtN[9], IrN_2[10], Re_2C[11], Re_2N[12], Re_3N[12], CrB_4[13] and WB_4[6,14–16]. Among them WB_4 exhibits the highest measured hardness with an asymptotic (i.e., load independent) hardness of about 30 GPa[6,14], which is attributed to its high content of boron that forms a three-dimensional covalent bond network that enhances its ability to resist shear deformation. However, the structural assignment of WB_4 was called into question by recent theoretical studies[17–20] that showed that the assigned WB_4 structure is unstable due to phonon softening and thus not viable. An alternative WB_3 structural model (space group: $P6_3/mmc$) was proposed based on calculated formation energy and a comparison with x-ray diffraction data. This issue, however, remains unsettled since more stringent tests of structure-property relation has not been performed to verify the proposed WB_3 structure. In fact, there is already a telltale sign indicating problems with the designation of the WB_3 structure: experiments show that the normalized c/a ratio of the synthesized WB_4 has a positive pressure dependence,[16] while the calculated elastic constants of WB_3 show[17,20] that $C_{11} > C_{33}$, which usually indicates a negative pressure dependence of the normalized c/a ratio. Furthermore, Vickers micro-indentation measurement indicates that the synthesized WB_4 has a load-independent asymptotic hardness (31.8, 28.1 GPa)[6,14] higher than that of ReB_2 (30.1, 26.6, 18.4 GPa)[3,6,7]. This property places the synthesized WB_4 atop the family of transition-metal light-element compounds for potential applications. It is therefore critical to make an accurate assessment of the (Vickers) indentation strength of the proposed WB_3 in comparison with that of ReB_2; it is expected to offer key insights to resolve the structural assignment, which is essential to further study of this family of materials.

In the present work, we report first-principles calculations of the ideal indentation strength of WB_3 and the isostructural MoB_3 using a recently developed method[21–24]. Our results show that under Vickers indentation WB_3 (and MoB_3) exhibits strength much lower than that of ReB_2, which is in direct contradiction to the experimental findings that synthesized WB_4 has an indentation hardness higher than that of ReB_2[3,6,7,14]. We also calculated the normalized c/a ratio of WB_3 and MoB_3, and the results indeed confirm the expected negative pressure dependence, which is again contrary to the experimentally observed pressure dependence for WB_4[16]. These results suggest that the proposed WB_3 structure is incompatible with the properties of the experimentally synthesized (nominal) WB_4 and that structural determination of the synthesized sample must be reopened for further study.

Recent advances in computation physics have made it possible to calculate the stress-strain relations of a perfect crystal in various shear deformation directions under the normal pressure beneath an indenter. The lowest shear peak stress under an indenter (i.e. ideal indentation strength) gives the stress at which a perfect crystal becomes mechanically unstable in indentation[21–24]. Ideal indentation strength provides a more accurate description for materials under indentation hardness tests than pure ideal shear strength that is calculated neglecting the normal pressure beneath

TABLE I: The calculated lattice constants (a, c) in Å, elastic constants C_{ij}, bulk modulus B in GPa and Poisson's ratio ν for WB_3 and MoB_3.

	a	c	C_{11}	C_{33}	C_{12}	C_{13}	C_{44}	B	ν
WB_3	5.20	6.31	646.88	478.23	85.52	171.92	278.64	291.55	0.16
MoB_3	5.21	6.30	622.78	430.38	85.09	156.90	252.30	273.14	0.156

the indenter[25–35]. While material strength and hardness are controlled by many factors, such as defect nucleation and mobility, ideal shear (indentation) strength calculations can predict incipient plasticity in a crystal[36] and determine the lowest shear stress needed to destabilize a perfect crystal, thus setting an upper bound for material strength. Measured strength of high quality samples can actually approach the calculated ideal strength[37,38]. This makes ideal shear (indentation) strength a benchmark quantity in assessing material strength and hardness; it is especially useful in a comparative study of different materials.

In this work, we performed calculations for ideal shear (indentation) strength under a Vickers indenter using the VASP code[39] and adopting the projector augmented wave (PAW) potentials[40] and generalized-gradient-approximation (GGA) for the exchange-correlation energy with a plane-wave basis set. The GGA-PBE exchange-correlation functional proposed by Perdew, Burke and Ernzerhof[41] was used. The total energy of the structure was minimized by relaxing the structural parameters using a conjugate gradient optimization method[42]. The total-energy and stress calculations used a hexagonal unit cell with a space group $P6_3/mmc$ for WB_3 and MoB_3. A $9\times9\times9$ Monkhorst-Pack[43] k-point grid and a 700 eV energy cutoff were used in the calculations. The energy convergence of the calculation is on the order of 1 meV per atom, with the residual stresses and forces in the fully relaxed structures less than 0.1 GPa and 0.001 eV/Å. The quasistatic ideal indentation strength and relaxed loading path were determined using a method described previously[21–24]. In this method, the shape of the (deformed) unit cell, the positions of the atoms and the relation between the shear stress σ_{xz} and shear strain ϵ_{xz} are determined completely at each step following a constrained atomic relaxation procedure, including the effect of the normal compressive pressure σ_{zz} by requiring that $\sigma_{zz} = \sigma_{xz}tan\Phi$ at each deformation step with Φ the centerline-to-face angle of the Vickers indenter. The lowest peak stress in all the indentation shear directions determines the ideal indentation strength of the structure, at which the crystal structure starts to destabilize. In a special case of setting $\sigma_{zz} = 0$, we recover the normal relaxation procedure used in previous calculations of pure ideal shear stresses[25–35] that neglect the effects of the normal compressive pressure beneath the indenter. As a test, we performed calculations for the equilibrium structures of WB_3 and MoB_3, and the obtained results of elastic constants, bulk moduli, and Poisson's ratios (see Table I) are all in good agreement with previously reported results[17,19,20].

We present in Fig. 1 the calculated stress-strain curves in various shear directions under pure and Vickers shear deformation for WB_3 and MoB_3. Detailed results on the calculated peak stresses and the corresponding strains at which the peak stresses appear are listed in Table II. From these results, it is clear that the weakest directions under

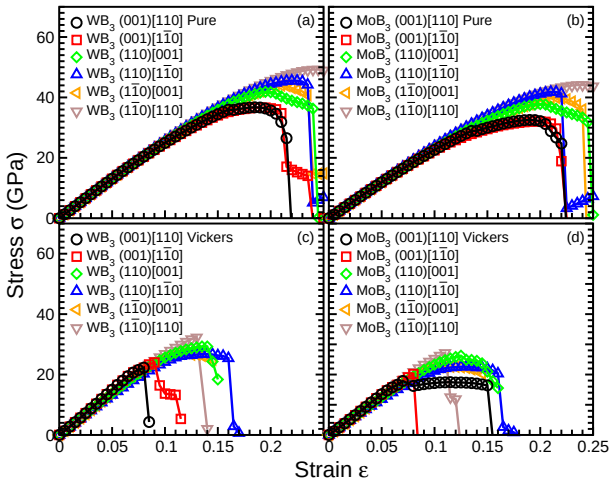

FIG. 1: (Color online) The calculated stress-strain curves in various shear directions under pure and Vickers shear deformations for WB_3 and MoB_3.

TABLE II: The calculated peak stress (σ_{max}) in GPa and corresponding strain (ϵ_{max}) in various directions under pure and Vickers shear deformation, as well the change of the peak stress under Vickers shear relative to that of pure shear ($\Delta\sigma_{max} = (\sigma^V_{max} - \sigma^P_{max})/\sigma^P_{max}$) for WB_3 and MoB_3.

WB_3	(001)[110]		(001)[1$\bar{1}$0]		(110)[001]		(110)[1$\bar{1}$0]		(1$\bar{1}$0)[001]		(1$\bar{1}$0)[110]	
	ϵ_{max}	σ_{max}	ϵ_{max}	σ_{max}	ϵ_{max}	σ_{max}	ϵ_{max}	σ_{max}	ϵ_{max}	σ_{max}	ϵ_{max}	σ_{max}
Pure	0.185	36.74	0.195	36.61	0.195	41.84	0.220	45.54	0.210	43.92	0.245	49.23
Vickers	0.080	22.27	0.090	24.00	0.135	29.30	0.135	26.81	0.12	27.12	0.130	32.28
$\Delta\sigma_{max}$	-39.4%		-34.4%		-30.0%		-41.1%		-38.3%		-34.4%	
MoB_3	(001)[110]		(001)[1$\bar{1}$0]		(110)[001]		(110)[1$\bar{1}$0]		(1$\bar{1}$0)[001]		(1$\bar{1}$0)[110]	
	ϵ_{max}	σ_{max}	ϵ_{max}	σ_{max}	ϵ_{max}	σ_{max}	ϵ_{max}	σ_{max}	ϵ_{max}	σ_{max}	ϵ_{max}	σ_{max}
Pure	0.190	32.55	0.195	32.07	0.200	37.82	0.215	41.84	0.215	39.92	0.240	44.13
Vickers	0.070	17.87	0.080	20.16	0.125	26.23	0.130	22.62	0.115	22.58	0.110	27.13
$\Delta\sigma_{max}$	-45.1%		-37.1%		-30.6%		-45.9%		-43.4%		-38.5%	

pure shear and (Vickers) indentation shear both appear in the (001) plane. A most notable feature contrasting the results under these two different loading conditions is that the pressure beneath the indenter produces considerable reductions in both the peak stresses and the corresponding peak strains. This result indicates a much earlier structural instability in WB_3 and MoB_3 under indentation compared to pure shear loading. It highlights the inadequacy of using pure shear strength to explain indentation hardness of tungsten borides[20]; this issue also applies to other transition-metal light-element compounds whose mechanical response is sensitive to loading conditions such as pressure beneath the indenter[24]. The lowest (Vickers) indentation shear stress peaks (i.e., the ideal indentation strength) of WB_3 and MoB_3 are 22.3 and 17.9 GPa, respectively, which are considerably lower than that of ReB_2 (27.6 GPa)[24]. The Vickers micro-indentation experiments show that the synthesized WB_4 has a measured load-independent asymptotic hardness (31.8, 28.1 GPa)[6,14] higher than that of ReB_2 (30.1, 26.6, 18.4 GPa)[3,6,7]. Our results indicate that the proposed WB_3 structure is incompatible with a key property of the synthesized (nominal) WB_4.

To understand the unexpectedly low indentation strength of WB_3 and MoB_3 compared to their pure shear strength, we calculated the structural and charge evolution with applied strain. We show in Fig. 2 the snapshots of WB_3 at equilibrium ($\epsilon = 0$) and in the weakest indentation shear direction (001)[110] under pure shear (neglecting the normal compressive pressure) at strain $\epsilon = 0.085$ and under (Vickers) indentation shear (including the normal compressive pressure) at $\epsilon = 0.08$ and $\epsilon = 0.085$ where the stress reaches its peak under indentation right before its sudden release [see Fig. 1(c)]. Also plotted in Fig. 2 are the electron localization functions (ELF) that give a local measurement of electron paring[44] on the (001) crystalline planes passing through the numbered atoms that were tracked during the structural evolution. The structural snapshots clearly show that, under indentation shear, normal pressure beneath the indenter induces a lateral expansion of the unit cell in the [1$\bar{1}$0] direction, causing the breaking up of the boron bonds (e.g., B_1-B_3, B_2-B_4, B_1-B_5 and B_2-B_6 bond) in the hexagonal lattices at strain ϵ=0.085, while under pure shear the boron hexagonal lattices remain intact at ϵ=0.085. In fact, results in Fig. 1(a) show that WB_3 is stable under pure shear in any direction when strain ϵ <0.2. The high-density valence electrons in the transition-metal light-element materials, such as WB_3, behave like a low-compressibility liquid. It is difficult to compress their volumes by hydrostatic pressure, which results in their high bulk moduli. However, in (Vickers) indentation hardness tests, apart from the shear deformation, the uniaxial normal compressive pressure beneath the indenter can cause a large lateral volume expansion of the valence electrons in these structures, which further stretches and weakens the (boron) atomic bonds in addition to that caused by the shear deformation in the indentation hardness test.

The same normal pressure induced lateral expansion and early breaking up of the boron bonds happens in MoB_3, even though its stress-strain relation in the weakest indentation shear direction (001)[110] is different from that of WB_3 [see Fig. 1(c,d)], suggesting that this is a common phenomenon in transition metal borides. In Fig. 3, we plot the calculated structural snapshots of MoB_3 at equilibrium ($\epsilon = 0$) and in the weakest indentation shear direction (001)[110] under pure shear at strain $\epsilon = 0.075$ and under (Vickers) indentation shear at $\epsilon = 0.07$ and $\epsilon = 0.075$ where the stress reaches its peak under indentation and then releases [see Fig. 1(d)]. Also plotted in Fig. 3 are the ELF on the (001) and (100) crystalline planes passing through the numbered atoms that were tracked. In MoB_3, the lateral expansion induced by the normal pressure breaks B_1-B_3 (B_2-B_4) bond which form three-center bonds[35] with the boron atoms in the neighboring boron layers (for instance, $\Delta B_1B_5B_8$), as indicated by the ELF on the (100) plane at strain $\epsilon = 0.075$. The capability of boron atoms to form both two- or three-center bonds[35] facilitates the structural transformation of transition-metal boride compounds with high boron contents under (indentation) deformations.

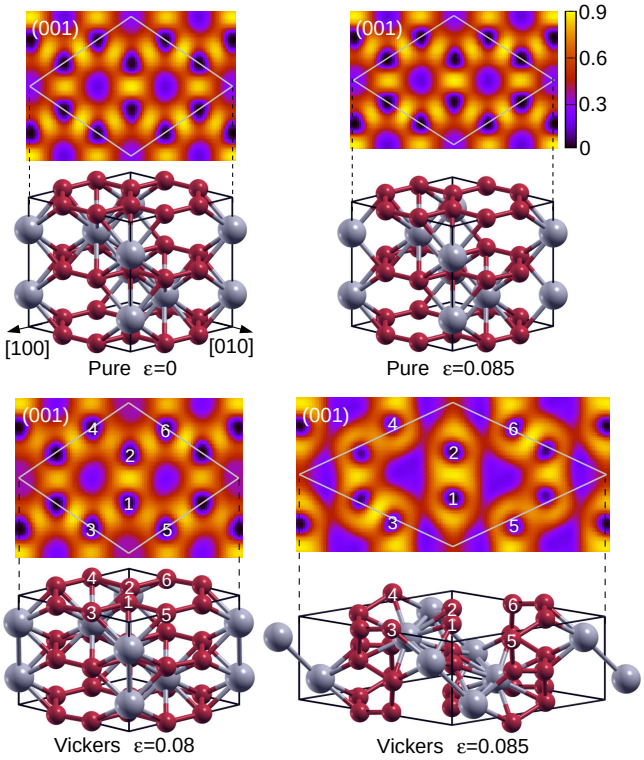

FIG. 2: (Color online) The calculated structural snapshots of WB_3 at equilibrium ($\epsilon = 0$) and in the (001)[110] shear direction under pure shear ($\epsilon = 0.85$) and Vickers shear ($\epsilon = 0.8$ and $\epsilon = 0.85$). Also show are the ELF on (001) planes passing through numbered atoms.

We note that the reduction of indentation strength from pure shear strength is much larger for WB_3 and MoB_3 compared to ReB_2.[24] This is attributed to a distinctive feature of the crystal structure of ReB_2, namely its buckled boron layers that can absorb the lateral bond and volume expansion by both flattening its buckled bond angles and stretching its bond lengths. In contrast, WB_3 and MoB_3 contain flat boron layers that can only stretch in the lateral expansion, resulting in much earlier bond breaking with lower indentation strength.

As an additional test of the recently proposed WB_3 structure[17–20], we calculated the normalized c/a ratio versus pressure compared to that of ReB_2 (see Fig. 4). The calculated results for ReB_2 agree well with experimental measurements[16]. Meanwhile, the results for WB_3 and MoB_3 show negative pressure dependence, which is consistent with their calculated elastic constants $C_{11} > C_{33}$ (see Table I). This is in stark contrast to experimental results for the synthesized WB_4 that show qualitatively different trends. Gu *et al.*[6] observed that the normalized c/a ratio of their WB_4 sample is almost equal to one under pressure up to 25 GPa; Liu *et al.*[15] found that the normalized c/a of their WB_4 sample decreases with pressure up to 25 GPa and then increases to one when pressure exceeds 35 GPa; and most recently Xie *et al.*[16], using neon as a better pressure transmitting medium, carefully measured the normalized c/a ratio of their WB_4 sample and found a positive pressure dependence up to 42 GPa followed by a quick decrease to less than one at higher pressure up to 60 GPa. These experimental results provide further support to the conclusion that the proposed WB_3 structure cannot explain the properties of the synthesized tungsten boride samples.

In summary, we have performed first-principles calculations to determine the stress-strain relation and the ideal indentation strength of WB_3 (and the isostructural MoB_3) that has been proposed as an alternative structural model for the recently synthesized (nominal) WB_4 samples reported in experiments. We find that the ideal indentation strength of WB_3 (and MoB_3) suffers an unusually large reduction (about 30%) compared to the corresponding pure ideal shear strength. The calculated ideal indentation strength of WB_3 (22.3 GPa) is considerably lower than that of ReB_2 (27.6 GPa), suggesting that the (asymptotic) Vickers hardness of WB_3 should be well below that of ReB_2. This result is in direct contradiction to the experimental findings that WB_4 has a hardness higher than that of ReB_2. Moreover, the calculated normalized c/a ratio of WB_3 (and MoB_3) exhibits negative pressure dependence, which is again in contradiction to the experimentally observed pressure dependence for the synthesized WB_4. These sharply contrasting results offer compelling evidence demonstrating that the proposed WB_3 structure is incompatible with key properties of the synthesized tungsten boride samples. The structural determination of the synthesized WB_4 is thus reemerging as an open question that deserves immediate attention.

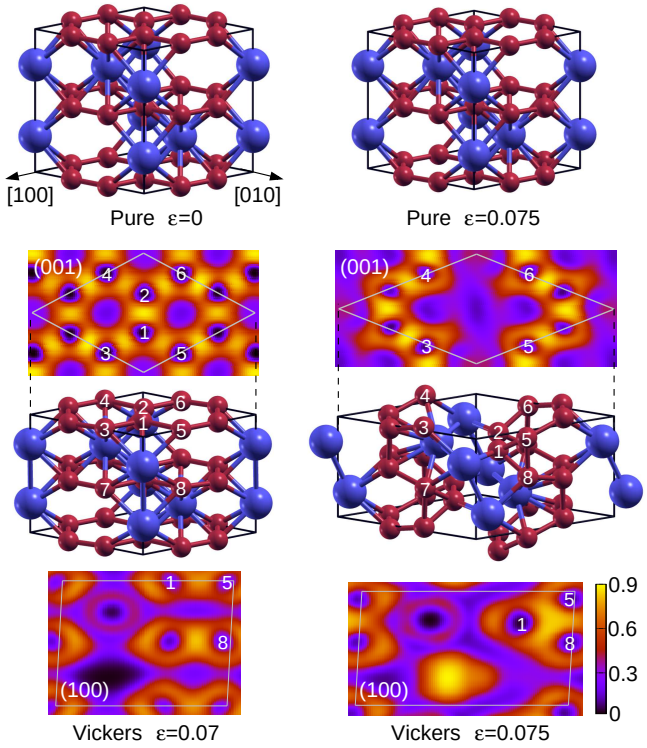

FIG. 3: (Color online) The calculated structural snapshots of MoB_3 at equilibrium ($\epsilon = 0$) and in the (001)[110] shear direction under pure shear ($\epsilon = 0.75$) and Vickers shear ($\epsilon = 0.7$ and $\epsilon = 0.75$). Also show are the ELF on (001) and (100) planes passing through numbered atoms.

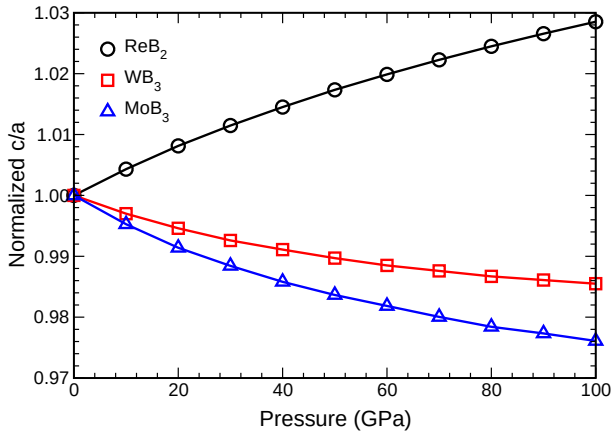

FIG. 4: (Color online) The calculated pressure dependence of the normalized c/a ratio of ReB_2, WB_3 and MoB_3.

This work was supported by DOE (DE-FC52-06NA26274) at UNLV and NNSF of China (No. 11174200) at SJTU. H. Sun appreciates the support of the Science and Engineering Interdisciplinary Research Foundation of SJTU.

* Corresponding author; Email:hsun@sjtu.edu.cn
† Corresponding author; Email:chen@physics.unlv.edu

[1] V. V. Brazhkin, A. G. Lyapin, and R. J. Hemley, Phil. Mag. A **82**, 231 (2002).
[2] R. B. Kaner, J. J. Gilman, and S. H. Tolbert, Science **308**, 1268 (2005).
[3] H. Y. Chung, M. B. Weinberger; J. B. Levine, A. Kavner, J. M. Yang, S. H. Tolbert, and R. B. Kaner, Science **316**, 436 (2007).
[4] J. B. Levine, S. L. Nguyen, H. I. Rasool, J. A. Wright, S. E. Brown, and R. B. Kaner, J. Am. Chem. Soc. **130**, 16953 (2008).
[5] A. Latini, J. V. Rau, D. Ferro, R. Teghil, V. R. Albertini, and S. M. Barinov, Chem. Mater. **20**, 4507 (2008).
[6] Q. Gu, G. Krauss, and W. Steurer, Adv. Mater. **20**, 3620 (2008).
[7] J. Q. Qin, D. W. He, J. H. Wang, L. M. Fang, L. Lei, Y. J. Li, J. A. Hu, Z. L. Kou, and Y. Bi, Adv. Mater. **20**, 4780 (2008).
[8] N. Orlovskaya, Z. L. Xie, M. Klimov, H. Heinrich, D. Restrepo, R. Blair, and C. Suryanarayana, J. Mater. Res. **26**, 2772 (2011).
[9] E. Gregoryanz, C. Sanloup, M. Somayazulu, J. Badro, G. Fiquet, H. K. Mao, and R. J. Hemley, Nat. Mater. **3**, 294 (2004).
[10] A. F. Young, C. Sanloup, E. Gregoryanz, S. Scandolo, R. J. Hemley, and H. K. Mao, Phys. Rev. Lett. **96**, 155501 (2006).
[11] Z. S. Zhao, L. Cui, L. M. Wang, B. Xu, Z. Y. Liu, D. L. Yu, J. L. He, X. F. Zhou, H. T. Wang, and Y. J. Tian, Cryst. Growth Des. **10**, 5024 (2010).
[12] A. Friedrich, B. Winkler, L. Bayarjargal, W. Morgenroth, E. A. Juarez-Arellano, V. Milman, K. Refson, M. Kunz, and K. Chen, Phys. Rev. Lett. **105**, 085504 (2010).
[13] H. Niu, J. Wang, X. Q. Chen, D. Li, Y. Li, P. Lazar, R. Podloucky, and A. N. Kolmogorov, Phys. Rev. B **85**, 144116 (2012)
[14] R. Mohammadi, A. T. Lech, M. Xie, B. E. Weaver, M. T. Yeung, S. H. Tolbert, and R. B. Kaner, PNAS **108**, 10958 (2011).
[15] C. Liu, F. Peng, N. Tan, J. Liu, F. Li, J. Qina, J. Wang, Q. Wang, and D. He, High Pressure Res. **31**, 275 (2011).
[16] M. Xie, R. Mohammadi, Z. Mao, M. M. Armentrout, A. Kavner, R. B. Kaner, and S. H. Tolbert, Phys. Rev. B **85**, 064118 (2012).
[17] Y. Liang, X. Yuan, and W. Zhang, Phys. Rev. B **83**, 220102(R) (2011).
[18] H. Gou, Z. Li, L. M. Wang, J. Lian, and Y. Wang, AIP Advances **2**, 012171 (2012).
[19] Y Liang, Z. Fu, X. Yuan, S. Wang, Z. Zhong, and W. Zhang, Europhys. Lett. **98**, 66004 (2012).
[20] R. F. Zhang, D. Legut, Z. J. Lin, Y. S. Zhao, H. K. Mao, and S. Veprek, Phys. Rev. Lett. **108**, 255502 (2012).
[21] Z. C. Pan, H. Sun, and C. F. Chen, Phys. Rev. Lett. **98**, 135505 (2007).
[22] Z. C. Pan, H. Sun, and C. F. Chen, Phys. Rev. B **79**, 104102 (2009).
[23] Z. C. Pan, H. Sun, Y. Zhang, and C. F. Chen, Phys. Rev. Lett. **102**, 055503 (2009).
[24] C. P. Zang, H. Sun, J. S. Tse, and C. F. Chen, Phys. Rev. B **86**, 014108 (2012).
[25] D. Roundy, C. R. Krenn, M. L. Cohen, and J. W. Morris Jr., Phys. Rev. Lett. **82**, 2713 (1999).
[26] H. Chacham and L. Kleinman, Phys. Rev. Lett., **85**, 4904 (2000).
[27] S. H. Jhi, S. G. Louie, M. L. Cohen, and J. W. Morris Jr., Phys. Rev. Lett. **87**, 075503 (2001).
[28] S. Ogata, J. Li, and S. Yip, Science **298**, 807 (2002).
[29] D. M. Clatterbuck, C. R. Krenn, M. L. Cohen, and J. W. Morris Jr., Phys. Rev. Lett. **91**, 135501 (2003).
[30] X. Blase, P. Gillet, A. S. Miguel, and P. Melinon, Phys. Rev. Lett. **92**, 215505 (2004).
[31] Y. Zhang, H. Sun, and C. F. Chen, Phys. Rev. Lett. **93**, 195504 (2004); Phys. Rev. Lett. **94**, 145505 (2005).
[32] M. G. Fyta, I. N. Remediakis, P. C. Kelires, and D. A. Papaconstantopoulos, Phys. Rev. Lett. **96**, 185503 (2006).
[33] J. Yang, H. Sun, and C. F. Chen, J. Am. Chem. Soc. **130**, 7200 (2008).
[34] P. Lazar, X. Q. Chen, and R. Podloucky, Phys. Rev. B **80**, 012103 (2009)
[35] W. Zhou, H. Sun and C. F. Chen, Phys. Rev. Lett. **105**, 215503 (2010).
[36] J. Li, K. J. Van Vliet, T. Zhu, S. Yip, and S. Suresh, Nature **418** 307 (2002).
[37] A. Gouldstone, H. -J. Koh, K. -Y. Zeng, A. E. Giannakopoulos, and S. Suresh, Acta Mater. **48**, 2277 (2000).
[38] C. R. Krenn, D. Roundy, M. L. Cohen, D. C. Chrzan, and J. W. Morris Jr., Phys. Rev. B **65**, 134111 (2002).
[39] See the web site: http://www.vasp.at/
[40] a) P. E. Blöchl, Phys. Rev. B **50**, 17953 (1994); b) G. Kresse and J. Joubert, Phys. Rev. B **59**, 1758 (1999).
[41] J. P. Perdew, K. Burke, and M. Ernzerhof, Phys. Rev. Lett. **77**, 3865 (1996).
[42] a) M. P. Teter, M. C. Payne, and D. C. Allan, Phys. Rev. B **40**, 12255 (1989); b) D. M. Bylander, L. Kleinman, and S. Lee, Phys Rev. B **42**, 1394 (1990).
[43] H. J. Monkhorst and J. D. Pack, Phys. Rev. B **13**, 5188 (1976).
[44] a) A. D. Becke, K. E. Edgecombe, J. Chem. Phys. **92**, 5397 (1990); b) B. Silvi, A. Savin, Nature **371**, 683 (1994).